Consensus Superiority of the Pharmacophore-Based Alignment, Over Maximum Common Substructure (MCS): 3D-QSAR Studies on Carbamates as Acetylcholinesterase Inhibitors

3 AUTHORS:

Shailendra Kumar Shrivastava

Samrat Ashok Technological Institute

7 PUBLICATIONS 113 CITATIONS

SEE PROFILE

Kuldeep Kumar Roy

University of Mississippi

22 PUBLICATIONS 208 CITATIONS

SEE PROFILE

Anil Kumar Saxena

Central Drug Research Institute

166 PUBLICATIONS 1,326 CITATIONS

SEE PROFILE

Consensus Superiority of the Pharmacophore-based Alignment, Over Maximum Common Substructure (MCS): 3D-QSAR Studies on Carbamates as Acetylcholinesterase Inhibitors

Shailendra S. Chaudhaery, Kuldeep K. Roy, and Anil K. Saxena*

Medicinal and Process Chemistry Division, Central Drug Research Institute, Lucknow, India-226001
*Corresponding author. Tel.: +91 522 2612412/ex4386; fax: +91 522 26123405
Email: anilsak@gmail.com
[a] CDRI Communication number 7712

Abstract

In view of the nonavailability of complete X-ray structure of carbamates co-crystallized with AChE enzyme, the 3D-QSAR model development based on co-crystallized conformer (CCBA) as well as docked conformer-based alignment (DCBA) is not feasible. Therefore, the only two alternatives *viz.* pharmacophore and maximum common substructure-based alignments are left for the 3D-QSAR comparative molecular field analyses (CoMFA) and comparative molecular similarity indices analyses (CoMSIA) model development. So, in the present study, the 3D-QSAR models have been developed using both alignment methods, where CoMFA and CoMSIA models based on pharmacophore-based alignment were in good agreement with each others and demonstrated significant superiority over MCS-based alignment in terms of leave-one-out (LOO) cross-validated q^2 values of 0.573 and 0.723 and the r^2 values of 0.972 and 0.950, respectively. The validation of the best CoMFA and CoMSIA models based on pharmacophore (Hip-Hop)-based alignment on a test set of 17 compounds provided significant predictive r^2 [$r^2_{pred(test)}$] of 0.614 and 0.788 respectively. The contour map analyses revealed the relative importance of steric, electrostatic and hydrophobicity for AChE inhibition activity. However, hydrophobic factor plays major contribution to the AChE inhibitory activity modulation which is in strong agreement with the fact that the AChE is having a wide active site gorge (~20Å) occupied by a large number of hydrophobic amino acid residues.

Keywords: Acetylcholinesterase, Carbamates, QSAR, CoMFA, CoMSIA, Pharmacophore.

INTRODUCTION

Alzheimer's disease (AD) is a progressive irreversible disorder of elderly patients which is characterized by widespread central cholinergic neuronal loss which, in turn, resulting in the loss of cognitive functions.[1] Two most significant histopathological hallmarks, found in the AD affected brain cells, are neuritic plaques and neurofibrillary tangles. To date, only symptomatic treatment approach has been proven to be effective in which cholinesterase (ChE) inhibitors are used to augment surviving cholinergic activity.[2-3] Two types of ChE enzyme are found in the Central Nervous System (CNS), acetylcholinesterase (AChE; EC 3.1.1.8) and butyrylcholinesterase (BChE). Both enzymes are able to catalyze the hydrolysis of acetylcholine (ACh) at a rate of >10,000 molecules per second.[4] The inhibition of AChE with reversible inhibitors[5] has been found to be one of the possible approach to restore acetylcholine (ACh) levels which is extensively reduced in the brain of AD patients. The enzyme, acetylcholinesterase (AChE), is responsible for the termination of impulse signaling at cholinergic synapses by catalyzing the hydrolysis of the neurotransmitter acetylcholine (ACh) and is also a promising drug-like target for the treatment of Alzheimer's disease. In fact it is one of the targets *viz.* AChE and N-methyl-D-aspartate (NMDA) that has provided few palliative drugs presently marketed for the treatment of Alzheimer's disease. These drugs include tacrine, galanthamine, donepezil, and rivastigmine as acetylcholinesterase inhibitors (AChEI) and memantine as a non-competitive NMDA antagonist for moderate improvement in memory and cognitive function.[5-12] The active site of AChE, located at the base of a long and narrow 20 Å gorge[13], consists of two sub sites, an "esteratic" sub site containing the catalytic machinery, and an "anionic" subsite responsible for binding the quaternary trimethylammonium tail group of ACh. The essential catalytic functional unit of AChE is the catalytic triad consisting of Ser203, His447, and Glu334 amino acid residues.[14] The oxyanion hole, formed by the peptidic NH groups of Gly121, Gly122 and Ala204 amino acid residues is another important functional unit in the esteratic sub site. It revealed that the acetyl head group of AChE directly involved in making and breaking bonds, is held in place by the oxyanion hole.[14] In the anionic sub-site, site-directed mutagenesis indicates that Trp86, Glu202, and Phe337 amino acid residues[14] play an important role in binding the quaternary trimethylammonium tail group.[15]

Structure-activity relationship (SAR) analyses is the basis for the perception of the structural features of both the inhibitors and the target receptors concerned in a particular biological process and thus helps in designing more effective inhibitors. SAR analysis can be done using computer-aided drug design (CADD) techniques which involves either of the two most commonly used techniques: the indirect/ligand-based drug design (LBDD) or the direct/structure-based drug design (SBDD) also known as structure based design. The latter has assumed increased importance due to rapid advances in the fields of structural and molecular biology. However, it appears relatively difficult to find a reliable predictive model based on the calculated energies obtained by docking.[16-17] To overcome this problem, highly predictive QSAR and CoMFA models are being developed using the technique of structure-based alignments. In our earlier studies on three most commonly used conformer-based alignments, namely, co-crystallized conformer-based alignment (CCBA), docked conformer-based alignment (DCBA), and global minima energy conformer-based alignment (GMCBA), it has been shown that the order of preference for the alignment selection for 3D QSAR model development may be CCBA > DCBA > GMCBA.[18] The complete X-ray structure of carbamates co-crystallized with AChE enzyme is not available because of the fact that the co-crystallized rivastigmine as well as ganstigmine are in broken form with carbamate part being covalently bound with the OH functionality of the Ser200 amino acid residue and rest non-carbamate part remains free in the active site of the AChE enzyme (Figure 1). Hence, the 3D-QSAR model development based on co-crystallized conformer (CCBA) as well as docked conformer-based alignment (DCBA) is not feasible. Since, the only possibility left in such case is to use the GMCBA and further, in view of our earlier findings where pharmacophore-

based alignment (PBA) has been shown to be suitable for 3D-QSAR model development, [16, 19,20] it appeared of interest to compare both the two alternatives *viz.* GMCBA and PBA for the 3D-QSAR model development using comparative molecular field analysis (CoMFA) and comparative molecular similarity indices analysis (CoMSIA).

In order to accomplish the above objective and to gain an insight into the main intermolecular interactions involved AChE inhibition at the molecular level, the following strategies were followed. First, a common feature pharmacophore model using Hip-Hop module of CATALYST[13] was developed using 12 carbamates as AChE inhibitors. It was followed by the selection of the best pharmacophore on the basis of the highest rank score which was then used for the conformational alignment of all 52 molecules[21,22] for 3D-QSAR model development.
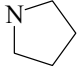
MATERIALS AND METHODS

Biological Data: 3D -QSAR studies were performed on structurally diverse set of 52 carbamates covering a good range of AChE inhibitory activity (Table 1).[21,22] The pharmacophore modeling using Hip-Hop algorithm implemented in the CATALYST software was carried out on a subset of 12 molecules with lowest-to-highest AChE inhibitory activity. The AChE inhibitory activity of the compounds, expressed in IC_{50} value in the nanomolar (nM) range, was transformed into $-\log IC_{50}$ (pIC_{50}) in order to make the normal distribution of the biological data for use in the present study.

Rational division of training and test sets: In view of the recent finding that q^2 appears to be the necessary but not the sufficient condition for the model to have a high predictive power,[23-24] the emphasis has been given for the validation on a test set. It has been suggested that the models should be tested on a sufficiently large test set (25-33% of total) to establish a reliable QSAR model.[24] Among several methods for the classification of the dataset into training and test sets *viz.* random sampling (RS), activity ranked clustering (ARC) and descriptor based clustering (DBC); the DBC has been shown to be the most effective method for selection of the representative test set (both in terms of activity and structural diversity).[5] Therefore, the dataset comprising 52 compounds was divided into training (35 compounds) and test (17 compounds) sets by DBC using molecular steric and electrostatic fields as descriptors. Hence, both the training and test sets covering a complete range of biological activity, physicochemical and structural features were used for the development and validation of the model respectively.

Table1: Structure and AChE inhibitory activities (nM) of the compounds

| | 1-14 | 15-18, 30 | 19-29 | 31-52 |

S.N.	R1	R2	NR3R4	X	Position of X	Y	Z	m	Activity IC50 (nM)
1≠	H	-	-	OCONMe2	6	O	4-NO2	-	8
2≠	H	-	-	OCONMe2	6	O	4-Cl	-	17
3	H	-	-	OCONMe2	7	O	4-NO2	-	10

4	H	-	-	$OCONMe_2$	7	O	4-Cl	-	219
5*≠	Me	-	-	$OCONMe_2$	6	O	4-NO_2	-	11
6*	Me	-	-	$OCONMe_2$	6	O	3Me, 4-NO_2	-	16
7≠	Me	-	-	$OCONMe_2$	6	O	3-NO_2	-	11
8*	Me	-	-	$OCONMe_2$	6	O	4-Cl	-	33
9	Me	-	-	$OCONMe_2$	6	O	4-F	-	49
10	Me	-	-	$OCONMe_2$	6	O	4-Br	-	34
11≠	Me	-	-	$OCONMe_2$	6	O	4-OMe	-	20
12≠	Me	-	-	$OCONMe_2$	5	O	4-NO_2	-	56
13	Me	-	-	$OCONMe_2$	7	O	4-NO_2	-	161
14	Me	-	-	$OCONMe_2$	7	O	4-Cl	-	265
15*	H	-	-	$OCONMe_2$	7	O	4-NO_2	-	55
16*	H	-	-	$OCONMe_2$	7	O	4Cl	-	215
17≠	Me	-	-	$OCONMe_2$	7	O	4-NO_2	-	61
18	Me	-	-	$OCONMe_2$	7	O	4-Cl	-	116
19	H	-	-	$OCONMe_2$	7	O	4-NO_2	-	92
20	H	-	-	$OCONMe_2$	7	O	3Me, 4-Cl	-	153
21≠	Me	-	-	$OCONMe_2$	7	O	4-NO_2	-	66
22*	Me	-	-	$OCONMe_2$	7	O	4-Me, 4-Cl	-	103
23	Me	-	-	$OCONMe_2$	7	O	4-Cl	-	139
24*	Me	-	-	$OCONMe_2$	7	O	4-F	-	135
25	Me	-	-	$OCONMe_2$	7	O	4-CF_3	-	285
26	Me	-	-	$OCONMe_2$	6	O	3-Me, 4-Cl	-	146
27≠	Me	Me	-	$OCONMe_2$	7	O	4-NO_2	-	60
28*	Me	Vinyl	-	$OCONMe_2$	7	O	4-NO_2	-	43
29*	Me	2-Thienyl	-	$OCONMe_2$	7	O	4-NO_2	-	150
30*	Me	Methylene	-	$OCONMe_2$	7	O	4-NO_2	-	27
31	-	-	NHMe	$OCONMe_2$	5	O	4-Cl	1	870
32	-	-	NHMe	$OCONMe_2$	5	O	4-F	1	870
33	-	-	NHMe	$OCONMe_2$	5	O	4-NO_2	1	221
34*	-	-	NHMe	$OCONMe_2$	6	O	4-OMe	1	220

4

35	-	-	NHMe	OCONMe$_2$	6	O	4-Me	1	726
36*	-	-	NHMe	OCONMe$_2$	6	O	H	1	341
37$^{\neq}$	-	-	NHMe	OCONMe$_2$	6	O	4-Cl	1	498
38*	-	-	NHMe	OCONMe$_2$	6	O	4-F	1	594
39	-	-	NHMe	OCONMe$_2$	6	O	4-CF$_3$	1	572
40	-	-	NHMe	OCONMe$_2$	6	O	4-CN	1	330
41$^{\neq}$	-	-	NHMe	OCONMe$_2$	6	O	2-NO$_2$	1	52
42$^{\neq}$	-	-	NHMe	OCONMe$_2$	6	O	3-NO$_2$	1	14
43	-	-	NHMe	OCONMe$_2$	6	O	4-NO$_2$	1	125
44*	-	-	NHMe	OCONMeH	6	O	4-NO$_2$	1	497
45*	-	-	NMe2	OCONMe$_2$	6	O	4-NO$_2$	1	319
46	-	-	NHEt	OCONMe$_2$	6	O	4-NO$_2$	1	326
47	-	-	NMeEt	OCONMe$_2$	6	O	4-NO$_2$	1	378
48	-	-		OCONMe$_2$	6	O	4-NO$_2$	1	852
49*	-	-	NHMe	OCONMe$_2$	6	O	4-NO$_2$	2	77
50	-	-	NHMe	OCONMe$_2$	6	NH	4-NO$_2$	1	36
51*$^{\neq}$	-	-	NHMe	OCONMe$_2$	6	S	4-NO$_2$	1	61
52	-	-	NHMe	OCONMe$_2$	6	-	4-NO$_2$	1	524

* indicates the test set compounds; $^{\neq}$ indicates compounds used for pharmacophore design using CATALYST/Hip-Hop module.

Modeling Tools: The pharmacophore modeling was accomplished using the Hip-Hop module implemented in CATALYST.[25] The 3D-QSAR studies (CoMFA[26,27] & CoMSIA[28-30]) were done on a Silicon Graphics Octane workstation using SYBYL 6.9 software.[31]

Methodology: The steps used in the development of 3D-QSAR model using the two strategies *viz.* Hip-Hop algorithm and MCS-based Alignment are outlined in figure
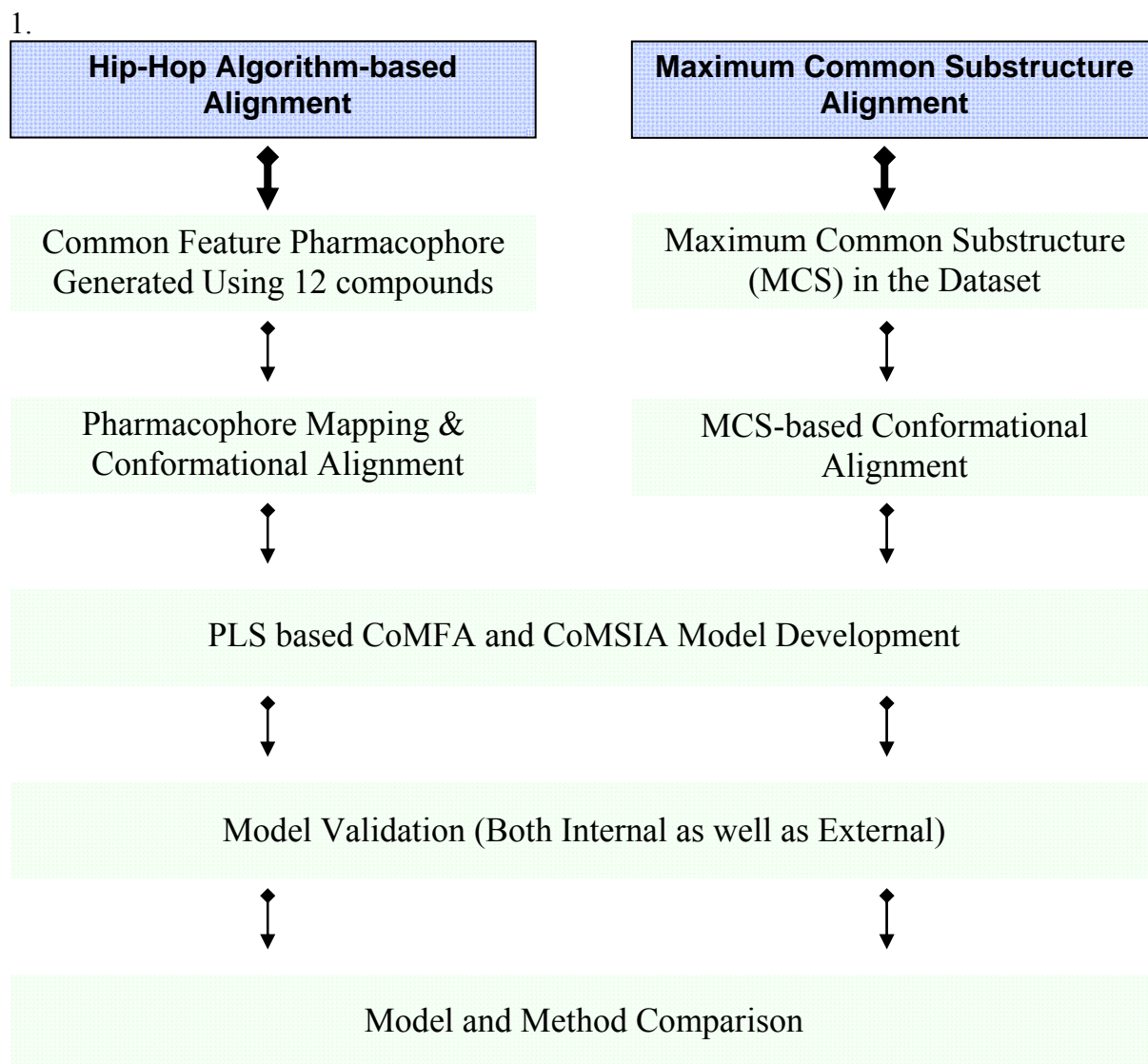
1.

Hip-Hop Algorithm-based Alignment	Maximum Common Substructure Alignment
↕	↕
Common Feature Pharmacophore Generated Using 12 compounds	Maximum Common Substructure (MCS) in the Dataset
↕	↕
Pharmacophore Mapping & Conformational Alignment	MCS-based Conformational Alignment
↕	↕
PLS based CoMFA and CoMSIA Model Development	
↕	↕
Model Validation (Both Internal as well as External)	
↕	↕
Model and Method Comparison	

Figure 1: Steps used in the 3D-QSAR model development using the two strategies.

Pharmacophore Modeling (Hip-Hop): Unlike CATALYST/HypoGen algorithm, Hip-Hop algorithm identifies features which are common among a set of compounds under study without considering their biological activities. Considering a collection of generated conformational models of molecules and chemical features selection as input, CATALYST produces a series of possible molecular alignments and then identifies 3D-configurations of features that are common to these set of molecules. The hypotheses are ranked based on (i) the number of molecules fitting the pharmacophore and (ii) the frequency of its occurrence (rank score). During common feature hypothesis generation, all of the possible chemical feature-based hypotheses possessing ten or lesser features are identified and ranked according to an estimate of their relative selectivity. The most selective hypothesis is given the highest numerical rank. The quality of the mapping between a compound and a hypothesis is indicated by the fit value. There are two control parameters employed in the Hip-Hop algorithm: *Principal* and *Maximum Omit Feat (MaxOmitFeat)*. The values of these control parameter *viz. principal* and *MaxOmitFeat* as input, set Hip-Hop algorithm to determine which molecule should be considered while building hypothesis space and which molecule should map to all or some of the features in the final hypothesis respectively.

All compounds were built using ISIS Draw 2.5, imported to Accelry's Discovery Studio window, and optimized using CHARMm force field. The CATALYST module treats molecular structures as templates consisting of strategically positioned chemical functions that will bind effectively with receptor. The biologically most important binding functions are deduced from a small set of compounds that cover a broad range of activity. CATALYST

generates conformational models for each compound using the Poling algorithm.[32,33] Diverse conformational models for each compound were generated such that the conformers covered accessible conformational space defined within 20 kcal/mol of the estimated global minimum. Among the two types of conformational analyses: fast and best quality provided in the CATALYST, the best option was used specifying 255 as maximum number of conformers and 20kcal/mol as energy cutoff. The estimation of the conformational energy was based on the CHARMm force field. The generated diverse conformations for molecules were submitted to CATALYST for hypothesis generation using Hip-Hop algorithm.

A set of 12 molecules as AChE inhibitors with lowest-to-highest AChE inhibitory activity were chosen as the input dataset in order to incorporate maximum diversity and minimum redundancy and to supply meaningful informations to the model generation process (CATALYST/Hip-Hop algorithm). In the pharmacophore model generation, the most active compound **1** ($IC_{50} = 8$ nM) was assigned a principal value of 2 and MaxOmitFeat value of 0 in the training set. Rest of the compounds was assigned a value of 1 for both control parameters. A set of ten pharmacophore hypotheses were generated from the training set of 12 compounds. During the initial phase of the hypothesis generation exercise, it was observed that four types of feature *viz.* HBA (Hydrogen bond acceptor), RA (Ring aromatic), positively ionizable (PI) and HY (Hydrophobic) were sufficient to map all critical chemical/structural features of all the training set molecules.

Conformational Sampling and Alignment: Structural alignment is perhaps the most subjective, yet critical, step in CoMFA study. The experience shows that the resulting 3D-QSAR models are often sensitive to a particular alignment scheme. However in contrast to CoMFA, CoMSIA is relatively less sensitive to changes in the orientation of the superimposed molecules in the lattice.[30] The reliability and efficiency of a CoMFA or CoMSIA results depend on the correct alignment of the input ligands. The pharmacophore mapping study is considered useful in the selection of both a proposed bioactive conformer and a superposition rule.[34] In the CATALYST; the studied molecules are automatically overlaid over the best pharmacorphore model and for each ligand, one aligned conformer based on the lowest RMS deviation of feature atom coordinates from those of the corresponding reference features are superimposed on the best hypothesis.

The relative alignment of the molecules is the most critical step in CoMFA and CoMSIA analyses which affects the final outcome; also the activity of the molecules is a result of the 3D disposition of features present in them or, in other words, their ability to assume a conformation for favorable interactions with the receptor. Therefore, the best hypothesis generated by Hip-Hop algorithm was used for the alignment of all the 52 compounds. The resulting alignment was then exported to SYBYL6.9 for CoMFA and CoMSIA studies. The partial charges for all the compounds were calculated using Gasteiger-Hückel method.

CoMFA and CoMSIA analyses: Unlike the traditional 2D-QSAR methods, which rely on the substituent parameters, the CoMFA exploits the active conformer and superposition rule for a set of molecules to provide quantitative correlation of the particular activity with the parameters in terms steric and electrostatic fields.[35]

The CoMFA[26,27] procedure can be summarized into three steps: (i) Firstly, all molecules under study are aligned using a molecular alignment methods *viz.* common-substructure based, multi-atom/point based (multi-fit), field-based (field-fit) and pharmacophore-based *etc*. (ii) Then, a 3D cubic lattice with a grid spacing of 2.0 Å in x, y and z directions are generated to enclose the molecule aggregate. (iii) A probe atom, e.g. sp^3 carbon with +1 or -1 charge, are placed at every lattice point to measure the electrostatic (Columbic with 1/r dielectric) or steric field (6–12 Lennard–Jones potential) by using molecular mechanics. To avoid too high and unrealistic energy values inside the molecule, a 30 kcal/mol as energy cutoff was applied. Finally, the results from the field samplings combined with the biological

7

activities of the molecules are put into a spreadsheat, and the partial least-squares (PLS) analysis is applied to get the final CoMFA model.

Another molecular modeling technique, CoMSIA,[28-30] is devised to overcome the problems associated with CoMFA of very rapidly changing steric fields near the atomic nuclei and scaling the two fields (steric and electrostatic) for PLS analyses. CoMSIA avoids the need of defining strict cutoff limits which can result in exclusion of several important data points and more interpretable contour maps. The CoMSIA is immune to small change in the relative orientation of the aligned molecules with respect to the lattice, which is another well-known problem in CoMFA. Moreover, in addition to the steric and electrostatic fields, the CoMSIA includes hydrogen bonds and hydrophobic interactions which are not sufficiently described by the steric and electrostatic fields and includes also an entropy component. In CoMSIA analyses, the standard settings (probe with charge +1, radius 1Å, hydrophobicity +1, hydrogen-bond donating +1, hydrogen-bond acceptor +1, attenuation factor α 0.3 and grid spacing 2.0 Å) were used to calculate five fields *viz.* steric, electrostatic, hydrophobic, acceptor and donor. CoMSIA calculates similarity indices at the intersections of a surrounding lattice. Similarity indices $A_{F,K}$ between the compounds of interest and a probe atom, systematically placed at the intersections of the lattice, are calculated according to equation 1 (e.g., at grid point q for molecule j of the data set)

$$A^q_{FK}(j) = -\sum_i \omega_{\text{probe},k}\ \omega_{ik}(e_{iq}^{-\alpha r})^2$$

……………………….. Eq^n-1

where i = the summation index over all atoms of the molecule j under investigation; ω_{ik} = the actual value of the physicochemical property k of atom i; $\omega_{\text{probe},k}$ = the probe atom with charge +1, α = the attenuation factor; and r_{iq} = the mutual distance between probe atom at grid point q and atom i of the test molecule. Large values of α will result in a strong attenuation of the distance-dependent consideration of molecular similarity.

Generally, a leave-one-out cross-validated r^2 (q^2) is used as a quantitative measure for CoMFA and CoMSIA model. The graphical representations (contours) of CoMFA and CoMSIA results are indicated by the regions where the variation in steric and electrostatic properties (in CoMFA) along with hydrophobic and hydrogen bonds (in CoMSIA) of different molecules in a data set are correlated with the variations in the biological activity.

Statistical Analyses/Partial Least Square (PLS): PLS was used to correlate the AChE inhibitory activity with the CoMFA and CoMSIA values containing magnitude of steric, electrostatic and other potentials. The generated models were assessed by using leave one out (LOO) cross-validation procedure by SAMPLS method as implied in SYBYL. A strict criterion for selection of optimal number of components was applied by selecting lowest PRESS value and also wherever the last added component increased q^2 less than 5%, the less complex model was chosen. In addition to LOO cross validation, the cross validation in groups using ten groups, repeating the procedure 10 times was also carried out. The mean of 10 readings is given as [$r^2_{cv\ (mean)}$]. The partial least-squares (PLS) algorithm was used to generate the final CoMFA and CoMSIA models with optimal number of components obtained using LOO cross-validation. The minimum standard deviation threshold was set at 2.0kcal/mol to speed up the analyses and to reduce the noise. The r^2_{cv} (q^2), PRESS, r^2, and SEE values were computed as defined in SYBYL6.9.

Predictive r^2: The predictive r^2 was based only on molecules (test set) which are not being considered in the training set. The predictive r^2 ($r^2_{pred(test)}$) value is defined as

$r^2_{pred(test)}$ = (SD - PRESS)/SD   …………………………………………………..Eq^n-2

where SD is the sum of squared deviation between the biological activities and the mean observed activity of the test set molecules and PRESS is the sum of squared deviations between the observed and the predicted activities of the test molecules.[36] Like r^2_{cv}, the predictive r^2 can assume a negative value reflecting a complete lack of predictive ability of

the model of the molecules included in the test set.[37] The robustness and statistical confidence of the derived models was further assessed by bootstrapping analyses (100 runs).

RESULTS AND DISCUSSION

Pharmacophore Modeling: A set of 12 compounds was used to generate 10 optimal hypotheses (Hypo) using the Hip-Hop module implemented in the CATALYST. The rank scores of these 10 optimal hypotheses were in the broad range of 247-232 (Table 2) indicative of greater probability of finding true correlation. Among these hypotheses shown in the descending order of rank score, the Hypo1 was found to be the best pharmacophore with the highest rank score of 246.97. It mapped all the important features of the most active compound and exhibited the highest fit value of 6.99 (Figure 2).
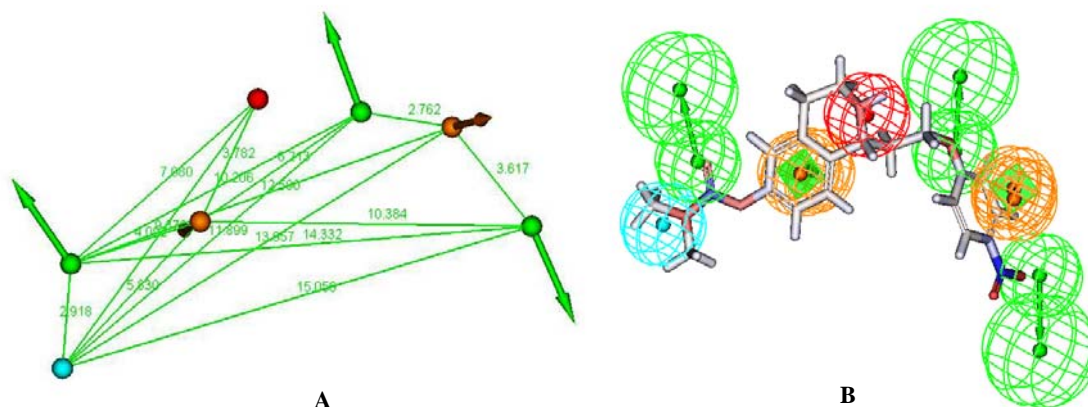

Figure **2**: (**A**) Common feature-based (Catalyst/Hip-Hop) pharmacophore model (Hypo1) with distance and angular constraints (**B**) mapping of the most active molecule 1 to Hypo1 with fit value of 6.99. [Hydrophobic (blue), hydrogen bond acceptor (green), ring aromatic (yellow) and positive ionizable (red) and the distance between chemical features are shown in Å]

The summary of the common feature pharmacophore hypothesis run is described in table 2. Since all hypotheses had the same 7 features *viz.* one hydrophobic (HY), three hydrogen bond acceptors (HBA 1-3), two ring aromatic (RA 1-2) and one Positive Ionizable (PI) features the Hypo-1 with the highest rank score was chosen for pharmacophore-based conformational alignment of 52 molecules. The figure 2A also depicts the distance and angular constraints between the features in the best pharmacophore (Hypo1). The conformation of the most active compound 1 superimposed on the best hypothesis (Hypo1) is shown in figure2B, where the carbonyl group of carbamate, the ethereal oxygen atom, and the nitro group substituted on phenyl ring were mapped as HBA 1, 2, and 3 respectively while the methyl substituent on carbamoyl nitrogen was mapped as hydrophobic feature and the two ring aromatic (RA-1, RA-2) features were mapped to the phenyl rings of 1,2,3,4 tetrahydroisoquinoline and side chain respectively.

Table 2: Summary of Common Feature Hypothesis Run using CATALYST/Hip-Hop

Hypo	Feature	Rank	Direct hit mask	Partial hit mask
1	RRPHAAA	246.97	DH: 111111111101	PH: 000000000010
2	RRPHAAA	245.67	DH: 111111111101	PH: 000000000010
3	RRPHAAA	241.11	DH: 111111111101	PH: 000000000010
4	RRPHAAA	237.94	DH: 111111111111	PH: 000000000000

9

5	RRPHAAA	237.00	DH: 111111111101	PH: 000000000010
6	RRPHAAA	235.05	DH: 111111111101	PH: 000000000010
7	RRPHAAA	235.01	DH: 111111111101	PH: 000000000010
8	RRPHAAA	234.48	DH: 111111111101	PH: 000000000010
9	RRPHAAA	234.45	DH: 111111111101	PH: 000000000010
10	RRPHAAA	232.23	DH: 111111111101	PH: 000000000010

R=Ring Aromatic, H=Hydrogen bond acceptor, Z=Hydrophobic, Y= Hydrophobic Aliphatic. Direct Hit=all the features are mapped. Direct Hit=1 means yes; Partial Hit= partial mapping of the hypothesis. Partial Hit=0 means no.

All 52 compounds were mapped onto Hypo-1 to obtain the pharmacophore-based molecular alignment (Figure 3) which was further used for the CoMFA and CoMSIA studies.
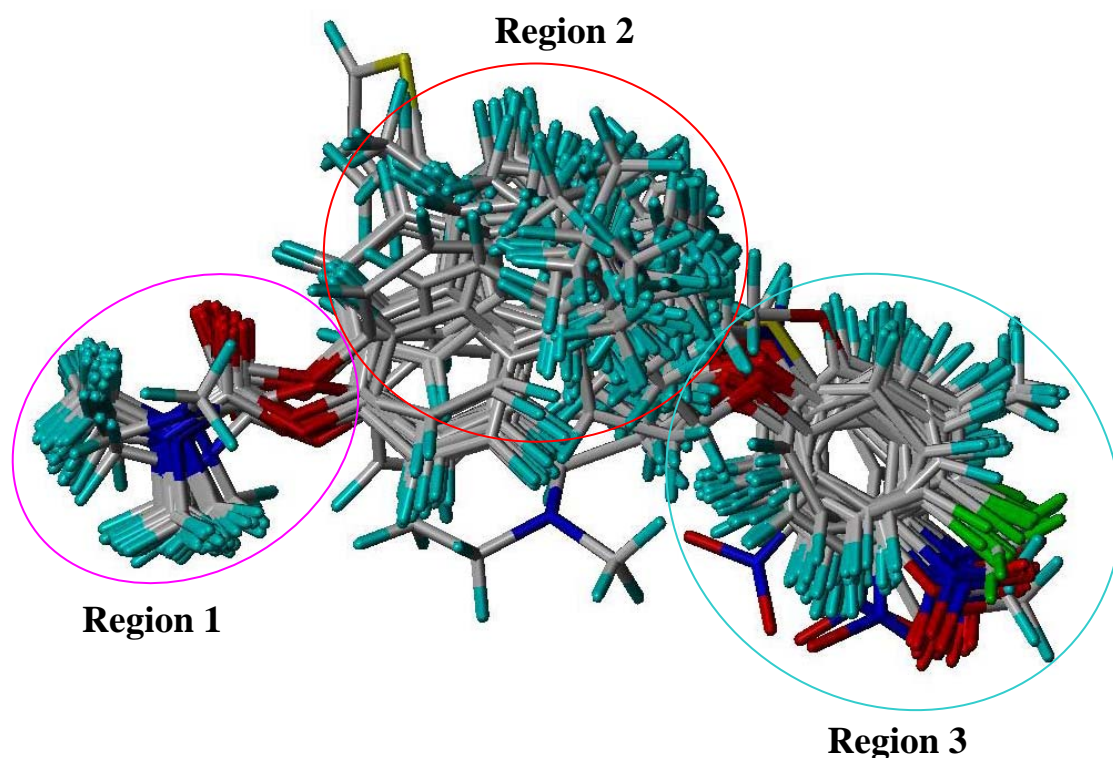

Figure 3: Hip-Hop algorithm-based conformational alignment of 52 AChE inhibitors with the important regions assigned namely as Region 1, 2, and 3.

Maximum Common Substructure (MCS)-based Alignment: This alignment approach is implemented in SYBYL6.9 along with other two alignment methods *viz.* multi-fit and field-fit methods. The first step of the MCS-based alignment is to explore the substructure which is common to the all molecules in the dataset. This is based on the assumption that the common substructure contributes equally to the biological activity of the molecules and can be assumed together as a constant. This is similar to the biophore concept implemented in APEX-3D system. The next step of the MCS-based alignment is to superimpose rest part of each molecule in such a way that the overall conformation of each molecule lie near to its local minima and the substituents of each molecule at a particular site used for major

10

modulations should be as closer as possible with respect to the rest of the molecules. This helps in focusing a particular region around the common substructure where major modulations have been made. This site is similar to that called as secondary site in APEX-3D system.

It has generally been observed that the maximum common substructure (MCS) should be rigid part where a few conformations are possible and flexible part should be ignored from consideration as MCS due to a large number of possible conformation and a large conformational energy space.

In our research work, the MCS-based molecular alignment was based upon a substructure shown in figure 4A and the generated molecular alignment in figure 4B.
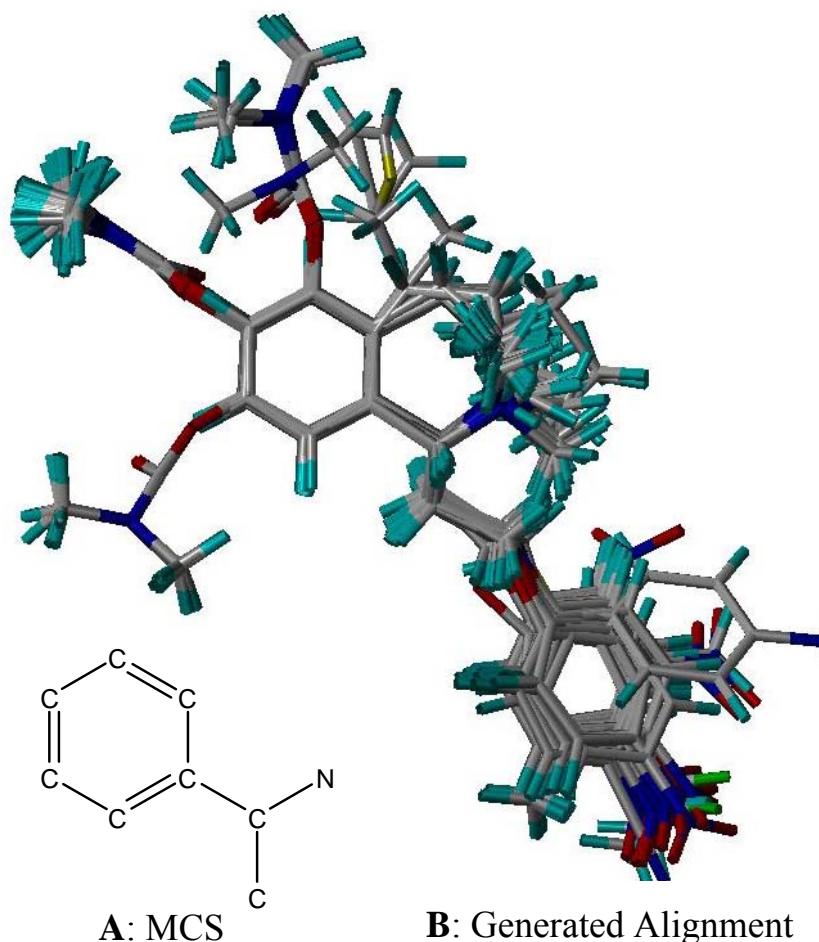

A: MCS   **B**: Generated Alignment

Figure 4: (**A**) Maximum Common Substructure (MCS) and (**B**) MCS-based molecular alignment

CoMFA Model and its Predictive Power: The final results of the CoMFA analyses with a 2.0 Å grid spacing, using above two alignments *viz*. Hip-Hop algorithm-based and MCS-based conformational alignment, are shown in table 3. The PLS analyses yielded consistent CoMFA results with the Hip-Hop algorithm-based alignment compared to MCS-based alignment as summarized in table 3. The optimal components that produced the best cross-validation linear regression coefficient were used to get the noncross-validated model. In 3D QSAR CoMFA and CoMSIA studies a q^2 of 0.3 is considered statistically significant[5,30] however a q^2 value of 0.4 is generally considered better. In view of it, the CoMFA models having $q^2 > 0.5$ were considered highly statistically significant. The LOO cross-validated PLS analysis resulted in a q^2 of 0.573 using five principal components. The noncross-validated PLS analysis using the same five principal components yielded an expected higher r^2 of 0.972 (SEE = 0.103). Although, the MCS-based alignment also provided a statistically significant LOO cross-validated q^2 of 0.568, it was found to be less viable in the prediction and explaining the diverse activity variations of the test set of 17 compounds with $r^2_{pred(test)} =$

0.497 only. The CoMFA model developed using the Hip-Hop algorithm-based alignment was found to be robust in predicting both the training as well as test set with r^2 of 0.972 and 0.614 respectively, thus indicating the superiority of the Hip-Hop-based alignment approach over MCS-based alignment. The observed and estimated AChE inhibitory activity (pIC_{50}) and the residual values for the training set and the test set, using the developed CoMFA model, are described in table 4 while the graphical plot between the observed vs estimated (predicted) AChE inhibitory activity for both training as well as test set is shown in figure 5.

Table 3: Summary of PLS Statistics of the best CoMFA and CoMSIA models based on Hip-Hop algorithm-based conformational alignment and MCS-based alignment of the training set of 35 molecules

Statistical Parameters		Hip-Hop algorithm-based alignment				MCS-based alignment			
		CoMFA (TS)	COMSIA			CoMFA (TS)	COMSIA		
			SEH	SEHA	SHA		SEH	SEHA	SHA
q^2		0.573	0.723	0.656	0.634	0.568	0.258	0.236	0.241
PRESS		0.404	0.319	0.361	0.373	0.405	0.513	0.523	0.511
r^2		0.972	0.950	0.948	0.957	0.954	0.583	0.475	0.445
SEE		0.103	0.135	0.141	0.127	0.131	0.385	0.425	0.437
F		202.624	143.520	105.151	130.470	121.411	14.428	14.487	12.819
N		5	4	5	5	5	3	2	2
Fraction	S	0.585	0.196	0.162	0.517	0.517	0.189	0.156	0.219
	E	0.415	0.476	0.332	0.483	0.483	0.359	0.265	-
	H	-	0.328	0.257	-	-	0.452	0.301	0.411
	A	-	-	0.247	-	-	-	0.277	0.370
r^2_{bs}		0.987	0.960	0.963	0.971	0.975	0.696	0.571	0.479
SD_{bs}		0.006	0.012	0.014	0.014	0.016	0.072	0.111	0.074
$r^2_{cv(mean)}$		0.566	0.700	0.621	0.584	0.546	0.245	0.227	0.160
$r^2_{pred(test)}$		**0.614**	**0.690**	**0.720**	**0.788**	**0.497**	**0.381**	**0.296**	**0.375**

q^2 = cross-validation correlation, PRESS= Predicted residual sum of squares; r^2 = regression coefficient; **SEE** = non cross-validated standard error of estimate; **F** = Fisher's F-value; **N** = optimal number of Components; r^2_{bs}= r^2 obtained after bootstrapping; SD_{bs}= bootstrapping standard deviation; $R^2_{cv(mean)}$ = mean r^2 of cross-validation in 10 groups; $r^2_{pred(test)}$ = predictive r^2; **S**=steric, **E**=electrostatic, **H**=hydrophobic field.

Table 4: Observed, Predicted AChE inhibitory activities (pIC_{50}) and residuals of the final CoMFA and CoMSIA models.

S.N.	Observed Activity (pIC_{50})	CoMFA (TS) Model		CoMSIA Model			
				SHA		SEHA	
		Predicted	Residual	Predicted	Residual	Predicted	Residual
$1^{\neq}$	-0.900	-0.816	-0.084	-0.738	-0.162	-0.706	-0.194
$2^{\neq}$	-1.230	-1.482	0.252	-1.419	0.189	-1.419	0.189
3	-2.000	-2.029	0.029	-1.955	-0.045	-2.098	0.098
4	-2.340	-2.276	-0.064	-2.431	0.091	-2.322	-0.018
$5^{*\neq}$	-1.040	-1.453	0.413	-1.219	0.179	-1.355	0.315
6*	-1.200	-0.992	-0.208	-1.100	-0.100	-1.021	-0.179
$7^{\neq}$	-1.040	-1.022	-0.018	-1.147	0.107	-1.201	0.161
8*	-1.520	-1.673	0.153	-1.765	0.245	-1.801	0.281
9	-1.690	-1.666	-0.024	-1.606	-0.084	-1.692	0.002

12

10	-1.530	-1.658	0.128	-1.636	0.106	-1.648	0.118
11$^{\neq}$	-1.300	-1.408	0.108	-1.283	-0.017	-1.347	0.047
12$^{\neq}$	-1.740	-1.630	-0.110	-1.582	-0.158	-1.624	-0.116
13	-2.200	-2.102	-0.098	-2.189	-0.011	-2.113	-0.087
14	-2.420	-2.419	-0.001	-2.456	0.036	-2.479	0.059
15*	-1.740	-1.648	-0.092	-1.584	-0.156	-1.531	-0.209
16*	-2.330	-1.893	-0.437	-1.912	-0.418	-1.956	-0.374
17$^{\neq}$	-1.780	-1.728	-0.052	-1.898	0.118	-1.911	0.131
18	-2.060	-2.058	-0.002	-1.997	-0.063	-1.879	-0.181
19	-1.960	-1.931	-0.029	-2.054	0.094	-2.136	0.176
20	-2.180	-2.108	-0.072	-1.993	-0.187	-2.028	-0.152
21$^{\neq}$	-1.810	-1.986	0.176	-2.054	0.244	-2.049	0.239
22*	-2.010	-2.275	0.265	-2.078	0.068	-2.231	0.221
23	-2.140	-2.192	0.052	-2.209	0.069	-2.280	0.140
24*	-2.130	-2.198	0.068	-1.957	-0.173	-2.140	0.010
25	-2.450	-2.389	-0.061	-2.404	-0.046	-2.285	-0.165
26	-2.160	-2.219	0.059	-2.096	-0.064	-2.354	0.194
27$^{\neq}$	-1.770	-1.710	-0.060	-1.684	-0.086	-1.613	-0.157
28*	-1.630	-1.969	0.339	-1.706	0.076	-1.766	0.136
29*	-2.170	-2.188	0.018	-2.066	-0.104	-2.136	-0.034
30*	-1.430	-1.678	0.248	-1.531	0.101	-1.509	0.079
31	-2.940	-2.920	-0.020	-2.984	0.044	-2.946	0.006
32	-2.940	-2.958	0.018	-2.964	0.024	-2.908	-0.032
33	-2.340	-2.442	0.102	-2.186	-0.154	-2.367	0.027
34*	-2.340	-1.881	-0.459	-2.224	-0.116	-2.290	-0.050
35	-2.860	-2.650	-0.210	-2.688	-0.172	-2.547	-0.313
36*	-2.530	-2.578	0.048	-2.742	0.212	-2.612	0.082
37$^{\neq}$	-2.690	-2.711	0.021	-2.617	-0.073	-2.653	-0.037
38*	-2.770	-2.261	-0.509	-2.397	-0.373	-2.304	-0.466
39	-2.750	-2.723	-0.027	-2.895	0.145	-2.769	0.019
40	-2.510	-2.380	-0.130	-2.362	-0.148	-2.381	-0.129
41$^{\neq}$	-1.710	-1.628	-0.082	-1.853	0.143	-1.674	-0.036
42$^{\neq}$	-1.150	-1.100	-0.050	-1.315	0.165	-1.153	0.003
43	-2.090	-2.003	-0.087	-2.080	-0.010	-2.124	0.034
44*	-2.690	-2.236	-0.454	-2.489	-0.201	-2.292	-0.398
45*	-2.500	-2.155	-0.345	-2.063	-0.437	-2.086	-0.414
46	-2.510	-2.666	0.156	-2.641	0.131	-2.666	0.156
47	-2.570	-2.571	0.001	-2.632	0.062	-2.543	-0.027
48	-2.930	-2.970	0.040	-2.823	-0.107	-2.899	-0.031
49*	-1.880	-1.817	-0.063	-1.868	-0.012	-1.876	-0.004
50	-1.550	-1.641	0.091	-1.461	-0.089	-1.480	-0.070
51*$^{\neq}$	-1.780	-1.394	-0.386	-1.405	-0.375	-1.395	-0.385

13

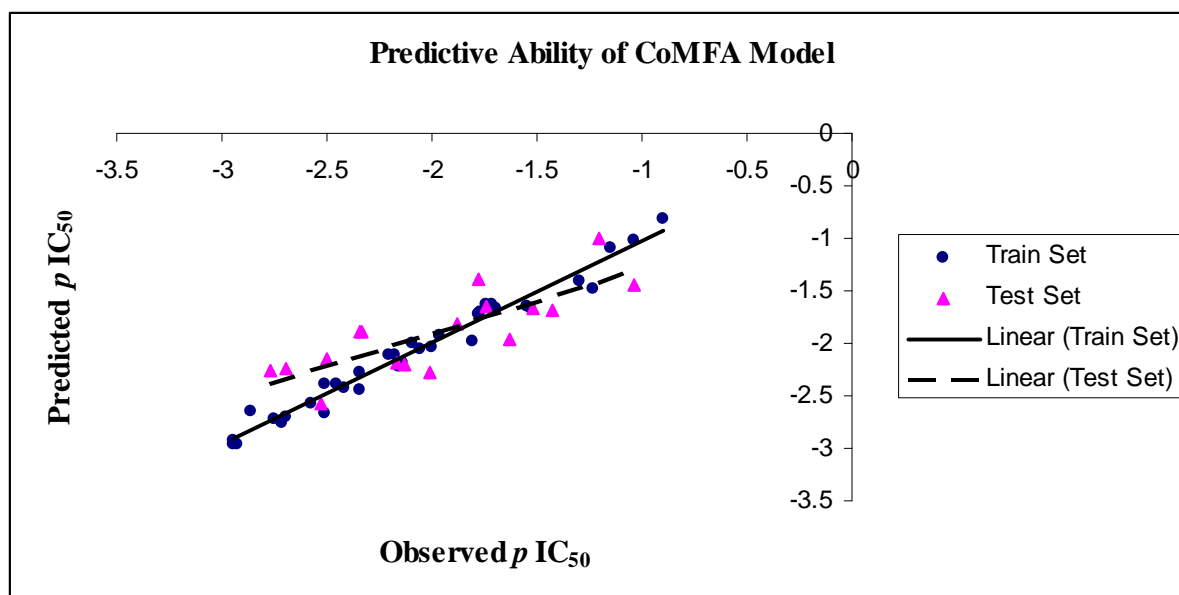| 52 | -2.710 | -2.760 | 0.050 | -2.620 | -0.090 | -2.654 | -0.056 |

Figure 5: The graph of observed versus predicted AChE inhibitory activities (pIC_{50}; nM) of both training set and test set compounds using the best CoMFA (TS) model.

CoMSIA Model and its Predictive Power: Various CoMSIA models were generated considering all possible combinations of CoMSIA field descriptors *viz.* steric (S), electrostatic (E), hydrophobic (H), donor (D) and acceptor (A). In the present study, steric, electrostatic, hydrophobic and acceptor field descriptors were found to play an important role in the modulation of AChE inhibitory activity and well explained the variation of AChE inhibitory activities among the studied carbamate-based inhibitors. The PLS analyses yielded consistent results of high statistical significance (Table 3) only with the alignment generated using CATALYST/Hip-Hop algorithm and the results obtained using the other alignment (MCS-based) were poor and far less significant which further strengthens the robustness of the CATALYST/Hip-Hop generated conformational alignment. This may be due to the fact that the Hip-Hop considers a large number of conformations of the active class of compounds, while in MCS, only the conformation near to its local minima of the most active molecule is considered. There were three best CoMSIA models based on Hip-Hop algorithm-based alignment which explained well the variation in AChE inhibitory activities for both the training as well as test set compounds. These three models were SEH, SEHA and SHA developed using S, E, H; S, E, H, A; and S, H, A field descriptors respectively. The PLS statistics of these three best CoMSIA models is summarized in table 3. The 'SEH' model gave the highest LOO cross-validated q^2 value of 0.723 (PRESS = 0.319) with four principal components and a noncross-validated r^2 of 0.950 (SEE = 0.135). The rest two CoMSIA models *viz.* 'SEHA' and 'SHA', gave slightly lesser value of LOO cross-validated q^2 of 0.656 (PRESS = 0.361) and 0.634 (PRESS = 0.373) respectively with five principal components and noncross-validated r^2 of 0.948 (SEE = 0.141) and 0.957 (SEE = 0.127) respectively using the same five principal components. In other words, in terms of the cross-validation q^2, the CoMSIA (SEH) model was found to be the best. However, on further validation of these three best CoMSIA models in respect of their ability to explain the activity variation among the test set of 17 compounds covering almost same range of AChE inhibitory activity, the model 'SHA' stood the best one with predictive r^2 [$r^2_{pred(test)}$] of 0.788, explaining about 80% variation in AChE inhibitory activity among the test set. The best found model, on the basis of q^2 that is the model 'SEH', explained about 70% variation in AChE inhibitory activity among the test set compounds with $r^2_{pred(test)}$ of 0.690 and the third model 'SEHA' gave a $r^2_{pred(test)}$ of 0.720 and also explained the activity variation by 72%. Therefore, in view of the

14

above, the model 'SHA' is not only the best among the three CoMSIA HipHop-based models but is also better than the CoMFA HipHop-based model. The AChE inhibitory activity (pIC$_{50}$), and the residual values for the training set and the test set compounds using the best CoMSIA (SHA) model, are given in table 4. The graphical plot of observed vs calculated AChE inhibitory activity for both training as well as test set is shown in figure 6.
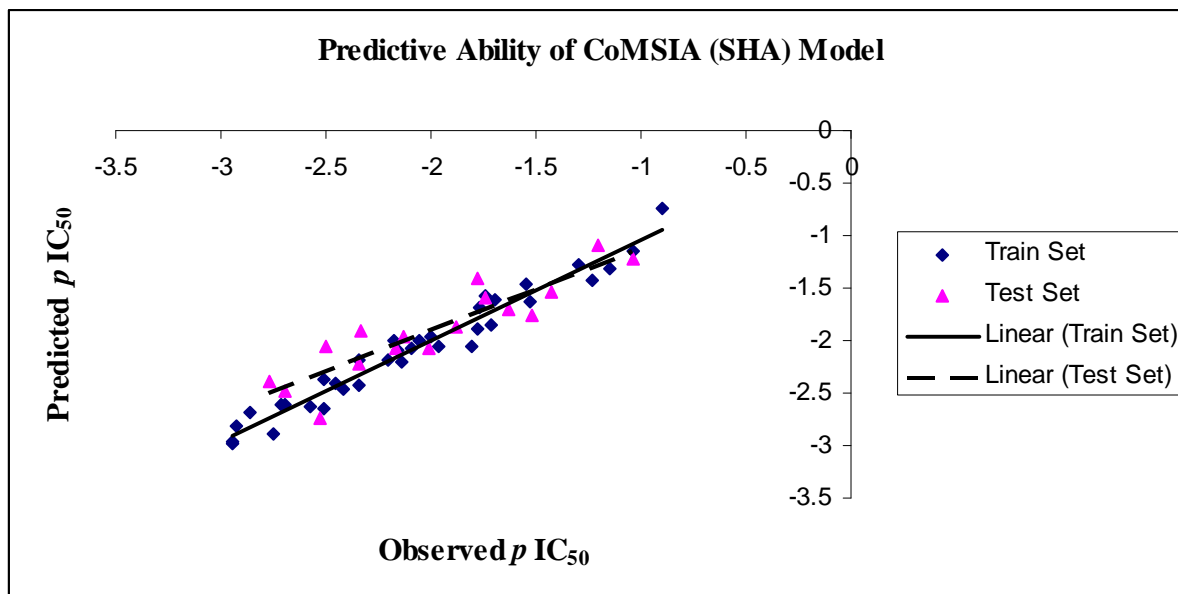

Figure 6: The graph of observed versus predicted AChE inhibitory activities (pIC$_{50}$; nM) of both training set and test set compounds using the best CoMSIA (SHA) model.

Graphical Interpretation of the CoMFA and CoMSIA Results: The CoMFA steric and electrostatic fields and additional hydrophobic and acceptor fields in case of CoMSIA obtained from the best CoMFA (TS) and CoMSIA (SHA) Hip-Hop-based models were plotted as 3D coloured contour maps (Figure 7). They are generated using the field type stdev*Coefficient to show the contribution for favourable and unfavourable interactions with the receptor in terms of steric (80% green, 20% yellow), electrostatic (80% blue and 20% red) and hydrophobic (80% yellow, 20% white). These contour maps show favourable/unfavourable regions where differences in molecular fields are associated with differences in biological activity.
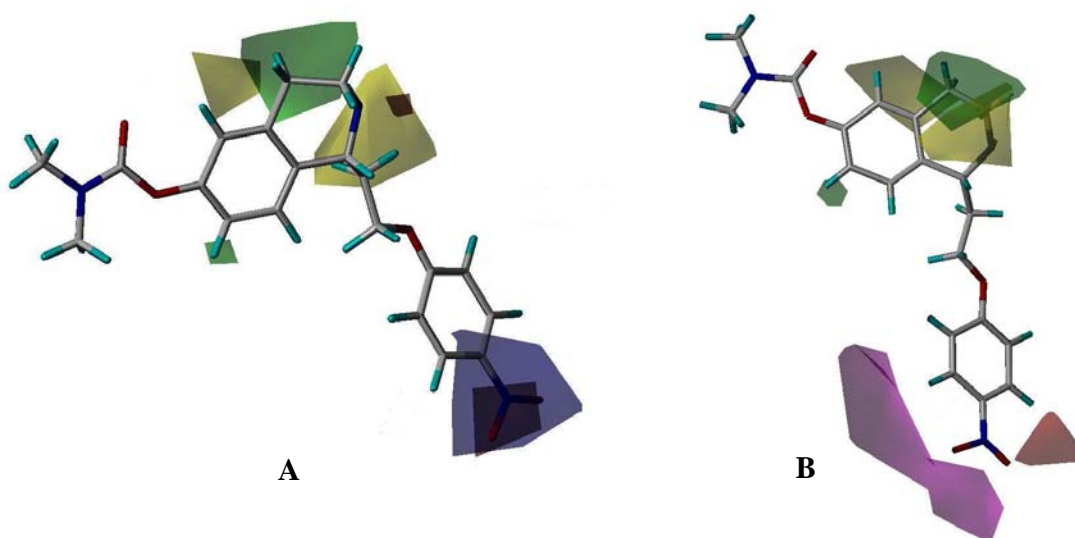
Figure 7: (**A**) CoMFA (TS) and (**B**) CoMSIA (stdev*coeff; SHA with hydrophobic contour hidden in this picture due to large polyhedron appeared for this hydrophobic field as shown in figure 10) around the most

potent AChE inhibitor. The favourable hydrophobic areas are indicated by yellow colour, whereas the disfavoured hydrophobic areas are shown by white colour. The favourable steric areas are shown in green, and the disfavoured steric areas are shown in yellow. The positive potential favoured areas are shown in blue, and the positive potential disfavoured areas are shown in red.

The steric interactions are represented by the green and yellow colours, while electrostatic interactions are represented by the red and blue colours (Figure 7 & 8). In the green regions of steric contour plot, the bulky substituent enhances biological activity, while the bulky substituent in the yellow regions is likely to decrease activity.

Both CoMFA and CoMSIA steric contours are almost similar. There was no contour map in the region 1 (Figure 7 & 8) because of the fact that CoMFA and CoMSIA attempt to represent those regions where structural/substituent modulations are being done. Since this carbamoyl part in region 1 (Figure 3) is same throughout the dataset. The CoMFA and CoMSIA steric contour map (Figure 8) revealed regions where steric factor play an important role as indicated by green and yellow polyhedra suggesting that more and less bulk respectively are needed in this region for enhancement of the activity.
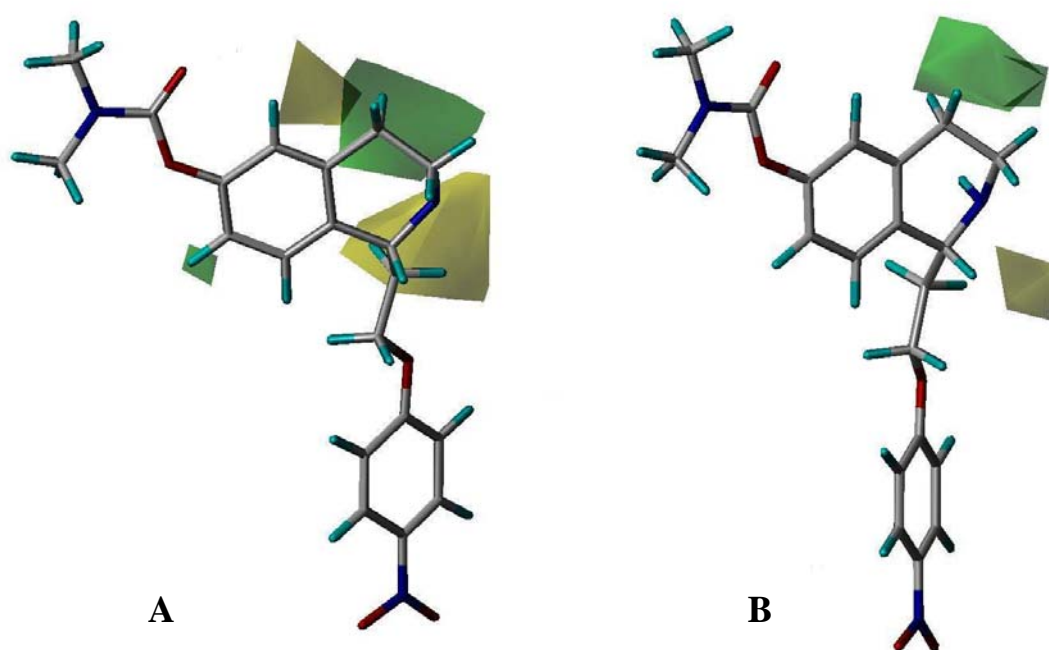
Figure 8 (A) CoMFA **(B)** CoMSIA (stdev*coeff) steric contour maps around the most active compound 1; The favorable steric areas are shown in green, and the disfavored steric areas are shown in yellow

Yellow contour maps, localized on the amine group (Figure 8A) in the region 2, suggest that the bulky substitution at the amino nitrogen was unfavorable for AChE inhibitory activity. This analysis is in the compliance with the observed AChE inhibitory activities in compounds **45** (NMe2, IC_{50}=319nM), **46** (NHEt, IC_{50}= 326nM), **47** (NMeEt, IC_{50}=378nM). A second yellow contour map (Figure 8A) around the position 5 of the aromatic ring in the region 2 (Figure 3) occupied by carbamate functionality in some compounds (**12**, **31-33**), indicated that substitution by the carbamates group at this position is not favorable for AChE inhibitory activity. The green contour embedded in the R_1 substitution on the olefin moiety (Region 2), suggested that an increase in bulky substitution at this position may lead to enhanced AChE inhibition activity. This analyses gave insight into the possible cause of why the compound **21**(R_1=H, IC_{50}=66nM) has a moderate activity in comparison to compounds **27** (R_1=Me, IC_{50}=60nM), **28** (R_1=vinyl, IC_{50}=43nM) respectively. Finally, these data are indicative of the specific steric requirements of the binding pocket of the hypothetical receptor.

In the electrostatic contour map, the red polyhedra represents regions where a negative charge is predicted to increase the activity of the compound whereas, the blue polyhedra represent regions where a positive charge or groups with lesser electron density may lead to enhancement in AChE inhibitory activity. The appearance of red coloured contours in the region 2 and 3 in both CoMFA and CoMSIA contours (Figure 9A&B) indicate that the high electron density (negative charge) imparted by suitable substitutions in these regions may lead to enhanced AChE inhibitory activity, whereas blue contours (appeared in region 3 only) indicated that groups with lesser electron density are more favourable in this region.
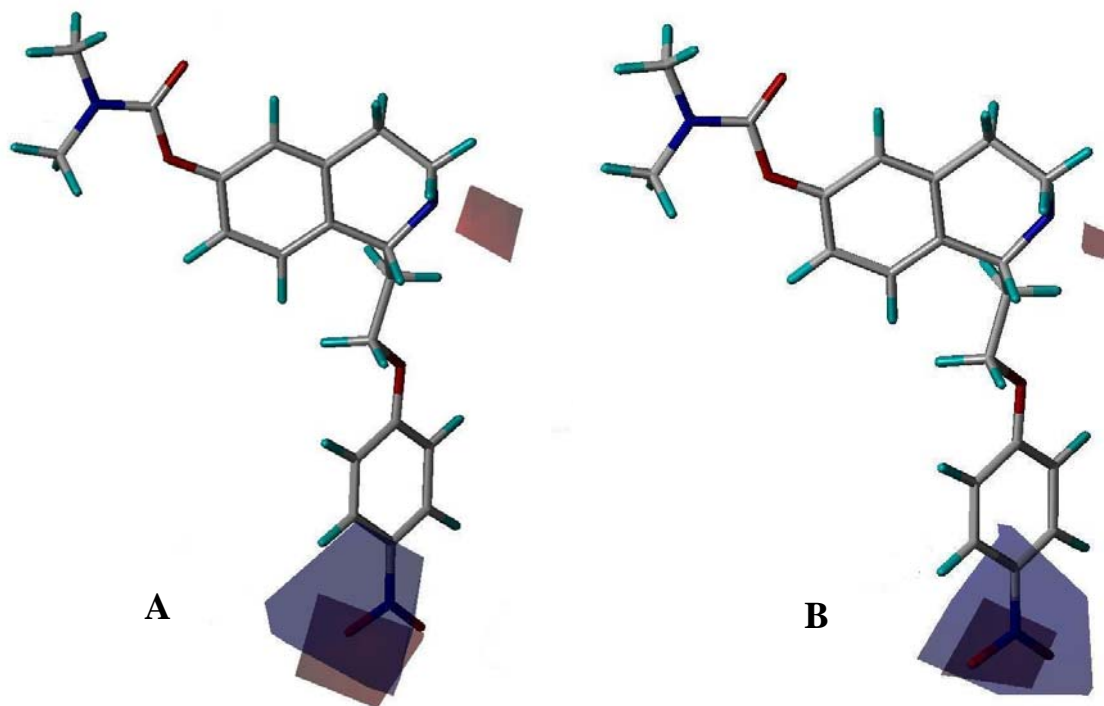
Figure 9: **(A)** CoMFA **(B)** CoMSIA (stdev*coeff) electrostatic contour plots around the most active compound **1**. The positive potential favored areas are shown in blue, and the positive potential disfavored areas are shown in red.

In CoMSIA hydrophobic contour map, the yellow coloured contours represent regions where an increase in hydrophobicity increases activity, whereas white coloured regions represent areas where increase in hydrophobicity decreases the biological activity. Hence, the observed yellow contours in the regions 2 and 3 (Figure 10) indicate that the substitutions in these regions by hydrophobic groups may lead to increased AChE inhibitory activity This analysis suggests that overall; the hydrophobicity of a molecule contributes effectively towards the potent inhibition of AChE enzyme. Non-appearance of white contour map in both CoMFA and CoMSIA contours (Figure **10**) further supports the above statements.
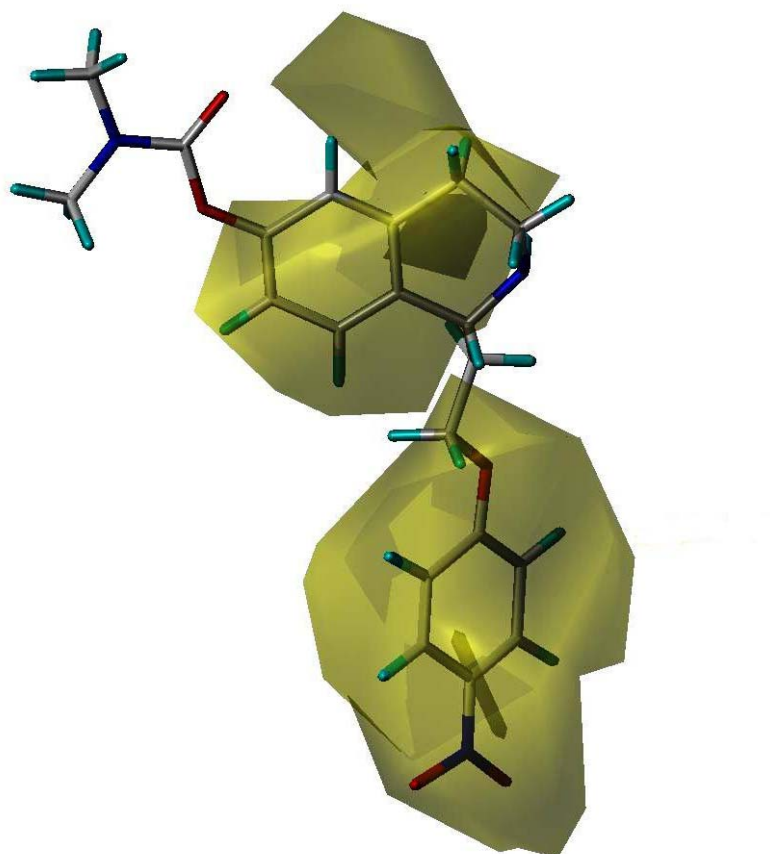
Figure 10: CoMSIA (stdev*coeff) hydrophobic contour around the most active compound **1**. The hydrophobic favored areas are represented by yellow polyhedra whereas the hydrophobic disfavored areas are represented by white polyhedra.

The probable binding orientation of the most active compound 1 in the active site gorge of the AChE enzyme generated using GOLD (version 3.0.1) is presented in Figure 11. The figure-11A shows the role of hydrophobic factor in the modulation of AChE inhibitory potential by the inhibitors. This analysis additionally supports the results obtained by the 3D-QSAR studies that the most of the interactions are hydrophobic in nature and the residues lying nearby the hydrophobic favorable areas mostly consist of hydrophobic amino acids (i.e., Gly, Val, and Leu). As depicted in figure 11A, the region 2 is placed in the hydrophobic pocket which is in strong agreement with the results obtained using 3D-QSAR studies represented by large yellow polyhedra (Figure 10). The figure-11B represents the importance of electrostatic factor in the modulation of AChE inhibitory potential by the inhibitors.
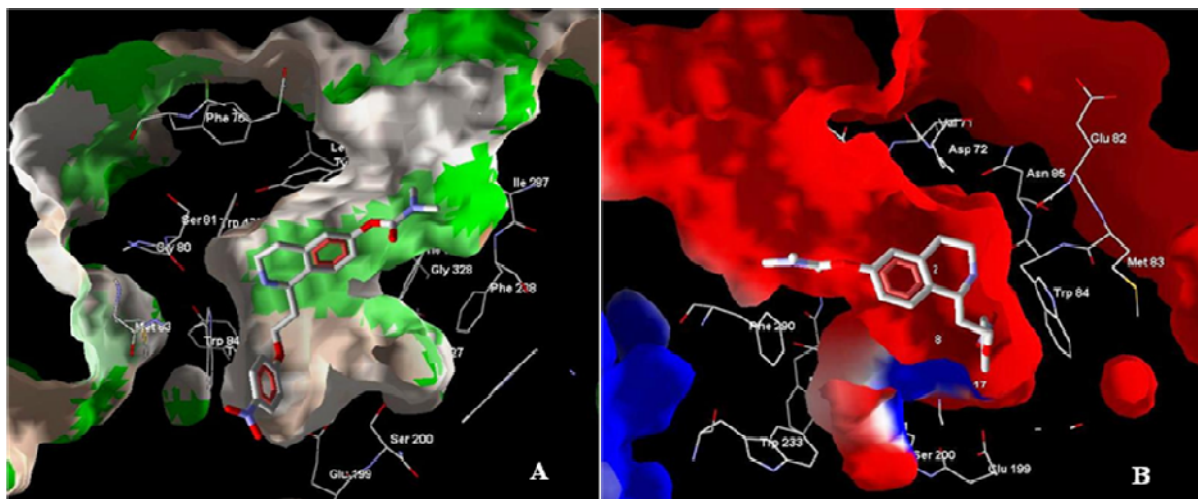
Figure 11: The docked bioactive conformation of the most active compound 1 into the active site of the AChE enzyme generated by GOLD (version 3.0.1). Representation of hydrophobic (**A**) and electrostatic (**B**) zones around the most active compound 1

CONCLUSION

In the present study, an attempt has been made to correlate AChE inhibitory activities of the diverse carbamates with steric, electrostatic, hydrophobic, donor and acceptor field descriptors.

In view of the nonavailability of complete X-ray structure of carbamates co-crystallized with AChE enzyme, the 3D-QSAR model development based on co-crystallized conformer (CCBA) as well as docked conformer-based alignment (DCBA) is not feasible. Therefore, the only two alternatives *viz.* pharmacophore and MCS-based alignments left for the 3D-QSAR comparative molecular field analyses (CoMFA) and comparative molecular similarity indices analyses (CoMSIA) model development have been considered in the present study, where, CoMFA and CoMSIA models based on pharmacophore-based alignment are in good agreement with each others and demonstrated significant superiority over MCS-based alignment in terms of leave-one-out (LOO) cross-validated q^2 values of 0.573 and 0.723 and the r^2 values of 0.972 and 0.950, respectively. The validation of the best CoMFA and CoMSIA models based on pharmacophore (Hip-Hop)-based alignment on a test set of 17 compounds has provided significant predictive r^2 [$r^2_{pred(test)}$] of 0.614 and 0.788 respectively. The contour map analyses revealed the relative importance of steric, electrostatic and hydrophobicity for AChE inhibition activity. However, hydrophobicity has been found to play a major role in the AChE inhibitory activity modulation which is in strong agreement with the fact that the AChE enzyme is composed of a wide active site gorge (~20Å) occupied by a large number of hydrophobic amino acid residues.

The results, together with the statistically significant correlations between the actual and predicted AChE inhibitory activities, demonstrated the power of common feature pharmacophore (Hip-Hop) algorithm-based conformational alignment scheme and proved superior over the MCS-based conformational alignment scheme implemented in SYBYL software. The studies suggest that in the development of 3D-QSAR models, the Hip-Hop-based alignment may be useful in getting the robust predictive models which may provide useful information required for proper understanding the important structural and physico-chemical features for designing novel AChE inhibitors comprising novel scaffolds leading to the candidate molecules as anti-dementia agents for drug development.

REFERENCES AND NOTES

(1) Butters, N.; Delis, D. C.; Lucas, J. A. Clinical assessment of memory disorders in amnesia and dementia. *Annu. ReV. Psychol.* **1995**, 46, 493–523.

(2) Giacobini, E. Cholinesterases: new roles in brain function and in Alzheimer's disease. *Neurochem. Res.* **2003**, 28, 515–522.

(3) Terry, A. V.; Buccafusco, J. J. The cholinergic hypothesis of age and Alzheimer's disease-related cognitive deficits: recent challenges and their implications for novel drug development. *J. Pharmacol. Exp. Ther.* **2003**, 306, 821–827.

(4) Bazelyansky, M.; Robey, E.; Kirsch, J. F. Fractional diffusion-limited component of reactions catalyzed by acetylcholinesterase. *Biochemistry* **1986**, 25, 125–130.

(5) Roy, K. K.; Dixit, A.; Saxena, A. K. An investigation of structurally diverse carbamates for acetylcholinesterase (AChE) inhibition using 3D-QSAR analysis. *Journal of Molecular Graphics and Modelling*, **2008**, 27, 197-208.

(6) Ballmaier, M.; Casamenti, F.; Scali, C.; Mazzoncini, R.; Zoli, M. Rivastigmine antagonizes deficits in prepulse inhibition induced by selective immunolesioning of cholinergic neurons in nucleus basalis magnocellularis. *Neuroscience* **2002**, 114, 91-98.

(7) Barnes, C. A.; Meltzer, J.; Houston, F.; Orr, G.; McGann, K. Chronic treatment of old rats with donepezil or galantamine: Effects on memory, hippocampal plasticity and nicotinic receptors. *Neuroscience* **2000**, 99, 17-23.

(8) Van Dam, D.; Abramowski, D.; Staufenbiel, M.; De Deyn, P. P. Symptomatic effect of donepezil, rivastigmine, galantamine and memantine on cognitive deficits in the APP23 model. *Psychopharmacology* **2005**, 180, 177-190.

(9) Clegg, A.; Bryant, J.; Nicholson, T.; McIntyre, L.; De Broe, S.; Gerard, K.;Waugh, N. Clinical and cost-effectiveness of donepezil, rivastigmine and galantamine for Alzheimer's disease: A rapid and systematic Review. *Health Technol. Assess.* **2001**, 5, 1-137.

(10) Clegg, A.; Bryant, J.; Nicholson, T.; McIntyre, L.; De Broe, S.; Gerard, K.; Waugh, N. Clinical and Cost-effectiveness of Donepezil, Rivastigmine and Galantamine for Alzheimer's disease. *Int. J. Technol. Assess. Health Care* **2002**, 18, 497-507.

(11) Goldlist, B.; Gordon, M.; and Naglie, G. Galantamine vs Donepezil in the treatment of Alzheimer's disease. *Drugs Aging* **2003**, 20, 1139-1140.

(12) Prasher, V. P. Review of donepezil: Ageing and health Issues in Intellectual Disabilities. *Int. J. Geriatr. Psychiatry* **2004**, 19, 509-515.

(13) Sussman, J. L.; Harel, M.; Frolow, F.; Oefner, C.; Goldman, A.; L, L. T.; Silman, I. Atomic structure of acetylcholinesterase from Torpedo californica: a prototypic acetylcholine-binding protein. *Science* **1991**, 253, 872-879.

(14) Ordentlich, A.; Barak, D.; Kronman, C.; Flashner, Y.; Leitner, M.; Segall, Y.; Ariel, N.; Cohen, S.; Velan, B.; Shafferman, A. Dissection of the human acetylcholinesterase active center determinants of substrate specificity. Identification of residues constituting the anionic site, the hydrophobic site, and the acyl pocket. *J. Biol. Chem.* **1993**, 268, 17083-17095.

(15) Radic, Z.; Gibney, G.; Kawamoto, S.; MacPhee-Quigley, K.; Bongiorno, C.; Taylor, P. Expression of recombinant acetylcholinesterase in a baculovirus system: kinetic properties of glutamate 199 mutants. *Biochemistry* **1992**, 31, 9760-9767.

(16) Prathipati, P.; Pandey, G.; Saxena, A. K. CoMFA and Docking Studies on Glycogen Phosphorylase a Inhibitors as Antidiabetic Agents. *J. Chem. Inf. Model.* **2005**, 45, 136-145.

(17) Cho, S. J.; Garsia, M. L.; Bier, J.; Tropsha, A. Structure-based alignment and comparative molecular field analysis of acetylcholinesterase inhibitors. *J. Med. Chem.* **1996**, 39, 5064–5071.

(18) Pandey, G.; Saxena, A. K. 3D QSAR Studies on Protein Tyrosine Phosphatase 1B Inhibitors: Comparison of the Quality and Predictivity among 3D QSAR Models Obtained from Different Conformer-Based Alignment.J. Chem. Inf. Model. **2006**, 46, 2579–2590.

(19) Enz, A.; Amstutz, R.; Boddeke, H.; Gmelin, G.; Malanowski, J. Brain selective inhibition of acetylcholinesterase: a novel approach to therapy for Alzheimer's disease. Prog. Brain Res. **1993**, 98, 431–438.

(20) Racchi, M.; Mazzucchelli, M.; Porrello, E.; Lanni, C.; Govoni, S. Acetylcholinesterase inhibitors: novel activities of old molecules. *Pharmacol. Res.* **2004**, 50, 441-445.

(21) Toda, N.; Tago, K.; Marumoto, S.; Takami, K.; Ori, M.; Yamada ,N.; Koyama, K.; Naruto, S.; Abe, K.; Yamazaki, R.; Hara, T.; Aoyagi, A.; Abe, Y.; Kaneko, T.; Kogen, H. Design, synthesis and structure–Activity relationships of dual inhibitors of acetylcholinesterase and serotonin transporter as potential agents for Alzheimer's disease. *Bioorg. Med. Chem.* **2003**, 11, 1935-1955.

(22) Toda, N.; Tago, K.; Marumoto, S.; Takami, K.; Ori, M.; Yamada, N.; Koyama, K.; Naruto, S.; Abe, K.; Yamazaki, R.; Hara, T.; Aoyagi, A.; Abe, Y. ; Kaneko, T.; Kogen, H. A Conformational Restriction Approach to the Development of Dual Inhibitors of Acetylcholinesterase and Serotonin Transporter as Potential Agents for Alzheimer's disease. *Bioorg. Med. Chem.* **2003**, 11, 4389-4415.

(23) Golbraikh, A.; and Tropsha, A. Beware of q^2!. *J. Mol. Graph. Model.* **2002**, 20, 269-276.

(24) Prathipati, P.; and Saxena, A. K. Comparison of MLR, PLS and GA-MLR in QSAR analysis. *SAR and QSAR in Environ. Res.* **2003**, 14, 433-446.

(25) CATALYST, release version 4.7; Accelrys, 9685 Scranton Road, San Diego, CA 92121.

(26) Wade, R. C. In *3D QSAR in Drug Design*; Kubinyi, H., Ed.; ESCOM: Leiden, 1993; pp 486-506.

(27) Wold, S.; Johansson, E.; Cocchi, M. In *3D QSAR in Drug Design*, Theory Methods and Applications; Kubinyi, H., Ed., ESCOM: Leiden, 1993; pp 523-550.

(28) Klebe, G.; Abraham, U.; Mietzner, T. Molecular similarity indices in a comparative analysis (CoMSIA) of drug molecules to correlate and predict their biological activity. *J. Med. Chem.* **1994**, 37, 4130-4146.

(29) Klebe, G.; Abraham, U. Comparative Molecular Similarity Index Analysis (CoMSIA) to study hydrogen-bonding properties and to score combinatorial libraries. *J. Comput.-Aided Mol. Des.* **1999**, 13, 1-10.

(30) Bohm, M.; Sturzebecher, J.; Klebe, G. Three-dimensional quantitative structure-activity relationship analyses using comparative molecular field analysis and comparative molecular similarity indices analysis to elucidate selectivity differences of inhibitors binding to trypsin, thrombin, and factor Xa. *J. Med. Chem.* **1999**, 42, 458-477.

(31) Tripos Inc. **1699**, South Hanley Road, St. Louis, MO 63144.

(32) Smellie, A.; Teig, S. L.; Towbin, P. Poling - promoting conformational variation. *J. Comput. Chem.* **1995**, 16, 171-187.

(33) Smellie, A.; Kahn, S. D.; Teig, S. L. Analysis of conformational coverage 0.1. Validation and estimation of coverage. *J. Chem. Inf. Comput. Sci.* **1995**, 35, 285-294.

(34) Martin, Y. C.; Bures, M. G.; Danaher, E. A.; DeLazzer, J.; Lico, I.; Pavlik, P. A. A fast new approach to pharmacophore mapping and its application to dopaminergic and benzodiazepine agonists. *J. Comput.- Aided Mol. Des.* **1993**, 7, 83-102.

(35) Cramer, R. D.; Patterson, D. E.; Bunce, J. D. Comparative Molecular Field Analysis (CoMFA). 1. Effect of shape on binding of steroids to carrier proteins. *J. Am. Chem. Soc.* **1988**, 110, 5959-5967.

(36) Waller, C. L.; Oprea, T. I.; Giolitti, A.; Marshall, G. R. Three- Dimensional QSAR of

21

Human Immunodeficiency Virus (I) Protease Inhibitors. 1. A CoMFA Study Employing Experimentally- Determined Alignment Rules. *J. Med. Chem.* **1993**, 36, 4152-4160.

(37) Cramer, R. D.; Bunce, J. D.; Patterson, D. E. Cross-validation, Bootstrapping, and Partial Least Squares Compared with Multiple Regression in Conventional QSAR Studies. *Quant. Struct.-Act. Relat.* **1988**, 7, 18-25.